CHEMISTRY OF MATERIALS
Article

Chem. Mater. **2010,** *22,* 557–564 557
DOI:10.1021/cm9030446

Palladium Nanoparticle Incorporation in Conjugated Microporous Polymers by Supercritical Fluid Processing

Tom Hasell, Colin D. Wood, Rob Clowes, James T. A. Jones, Yaroslav Z. Khimyak, Dave J. Adams, and Andrew I. Cooper*

Department of Chemistry and Centre for Materials Discovery, University of Liverpool, Crown Street, Liverpool L69 7ZD, United Kingdom

Received October 1, 2009. Revised Manuscript Received December 8, 2009

Palladium nanoparticles have been dispersed uniformly throughout a microporous poly(aryleneethynylene) material by the infusion of a CO_2-soluble Pd precursor. The resulting composite has good thermal stability and has potential applications for example in heterogeneous catalysis. The porosity of the polymeric support was maintained after inclusion of the metal and the hydrogen uptake at room temperature was increased with respect to the unloaded porous support.

1. Introduction

Microporous materials are of interest because of their potential application in areas such as gas sorption, separation, and heterogeneous catalysis.[1] Materials investigated for such applications include zeolites,[2] metal organic frameworks (MOFs),[3] covalent organic frameworks (COFs),[4] activated carbons,[5] polymers of intrinsic microporosity (PIMs),[6] and hyper-cross-linked polymers (HCPs).[7]

The fusion of porous materials research and nanoparticle technology has been a fruitful area of interdisciplinary research.[8] Metal nanoparticles have unique properties that depend on their size, shape, and degree of dispersion. The embedding of nanoparticles into porous supports offers potential for particle size control as well as protecting and stabilizing the nanoparticles for use in applications.

Distributing metal nanoparticles within a high surface area support is of interest for a number of reasons. For example, the use of supported metal nanoparticles has been suggested to enhance hydrogen uptake for gas storage by "spillover" mechanisms,[9] although the mechanism of this is highly disputed. Other potential key applications include heterogeneous catalysis[10] and surface-enhanced Raman spectroscopy (SERS).[11] All of these applications require the distribution of small, well-defined nanoparticles over a stable and inert solid support. For example, it was suggested that the degree of Pd−carbon contact, pore size, and the state of the hydrogen receptor surface are significant factors in contributing to enhanced hydrogen spillover.[12] Enhanced H_2 uptake in the presence of transition metal nanoparticles with nearly filled *d*-shells (Pt, Pd, Ni) has been reported.[13]

The synthesis of suitable hydrogen storage materials is a key challenge in the development of a hydrogen economy. Recent research interest has focused on the development of nanostructured porous and high surface area materials for this application.[14] Hydrogen storage by spillover has

*Corresponding author. E-mail: aicooper@liverpool.ac.uk.

(1) Schüth, F.; Sing, K. S. W.; Weitkamp, J. *Handbook of Porous solids*; Wiley VCH: Heidelberg, Germany, 2002.
(2) Caro, J.; Noack, M.; Kolsch, P.; Schafer, R. *Microporous Mesoporous Mater.* **2000**, *38*(1), 3–24.
(3) (a) Yaghi, O. M.; Li, H. L.; Davis, C.; Richardson, D.; Groy, T. L. *Accounts Chem. Res.* **1998**, *31*(8), 474–484. (b) Cheetham, A. K.; Ferey, G.; Loiseau, T. *Angew. Chem., Int. Ed.* **1999**, *38*(22), 3268–3292. (c) Kitagawa, S.; Kitaura, R.; Noro, S. *Angew. Chem., Int. Ed.* **2004**, *43*(18), 2334–2375.
(4) (a) Cote, A. P.; Benin, A. I.; Ockwig, N. W.; O'Keeffe, M.; Matzger, A. J.; Yaghi, O. M. *Science* **2005**, *310*(5751), 1166–1170. (b) El-Kaderi, H. M.; Hunt, J. R.; Mendoza-Cortes, J. L.; Cote, A. P.; Taylor, R. E.; O'Keeffe, M.; Yaghi, O. M. *Science* **2007**, *316*(5822), 268–272.
(5) Villar-Rodil, S.; Suarez-Garcia, F.; Paredes, J. I.; Martinez-Alonso, A.; Tascon, J. M. D. *Chem. Mater.* **2005**, *17*(24), 5893–5908.
(6) (a) McKeown, N. B.; Makhseed, S.; Budd, P. M. *Chem. Commun.* **2002**, No. 23, 2780–2781. (b) McKeown, N. B.; Hanif, S.; Msayib, K.; Tattershall, C. E.; Budd, P. M. *Chem. Commun.* **2002**, No. 23, 2782–2783. (c) Carta, M.; Msayib, K. J.; Budd, P. M.; McKeown, N. B. *Org. Lett.* **2008**, *10*(13), 2641–2643. (d) McKeown, N. B.; Budd, P. M.; Msayib, K. J.; Ghanem, B. S.; Kingston, H. J.; Tattershall, C. E.; Makhseed, S.; Reynolds, K. J.; Fritsch, D. *Chem.—Eur. J.* **2005**, *11*(9), 2610–2620.
(7) (a) Lee, J. Y.; Wood, C. D.; Bradshaw, D.; Rosseinsky, M. J.; Cooper, A. I. *Chem. Commun.* **2006**, No. 25, 2670–2672. (b) Wood, C. D.; Tan, B.; Trewin, A.; Niu, H. J.; Bradshaw, D.; Rosseinsky, M. J.; Khimyak, Y. Z.; Campbell, N. L.; Kirk, R.; Stockel, E.; Cooper, A. I. *Chem. Mater.* **2007**, *19*(8), 2034–2048. (c) Davankov, V. A.; Tsyurupa, M. P., Angew. Makromol. Chem. **1980**, *91* (NOV), 127−142; (d) Davankov, V. A.; Tsyurupa, M. P. *React. Polym.* **1990**, *13*(1-2), 27–42.
(8) White, R. J.; Luque, R.; Budarin, V. L.; Clark, J. H.; Macquarrie, D. J. *Chem. Soc. Rev.* **2009**, *38*(2), 481–94.
(9) Wang, L. F.; Yang, R. T. *Energy Environ. Sci.* **2008**, *1*(2), 268–279.
(10) (a) Aiken, J. D.; Finke, R. G. *J. Mol. Catal.* **1999**, *145*(1-2), 1–44. (b) Jiang, J. X.; Su, F.; Trewin, A.; Wood, C. D.; Niu, H.; Jones, J. T. A.; Khimyak, Y. Z.; Cooper, A. I. *J. Am. Chem. Soc.* **2008**, *130*(24), 7710–7720.
(11) Xiong, Y. J.; McLellan, J. M.; Chen, J. Y.; Yin, Y. D.; Li, Z. Y.; Xia, Y. N. *J. Am. Chem. Soc.* **2005**, *127*(48), 17118–17127.
(12) Bhat, V. V.; Contescu, C. I.; Gallego, N. C. *Nanotechnology* **2009**, *20* (20), 204011−204021.
(13) Contescu, C. I.; Brown, C. M.; Liu, Y.; Bhat, V. V.; Gallego, N. C. *J. Phys. Chem. C* **2009**, *113*(14), 5886–5890.
(14) Morris, R. E.; Wheatley, P. S. *Angew. Chem., Int. Ed.* **2008**, *47*(27), 4966–4981.

© 2009 American Chemical Society
Published on Web 12/23/2009

been suggested as a promising approach to enhancing the ambient-temperature hydrogen storage capacity of nanostructured materials including carbon nanostructures, zeolites, MOFs and COFs.[15] Conceptually, spillover involves the dissociation of hydrogen molecules on metal nanoparticles followed by subsequent hydrogen atom migration onto the nearby substrate by spillover and surface diffusion.[15b,16] Although the precise details of these processes are unclear, it seems that adsorption, diffusion, and the overall qualitative behavior of hydrogen spillover systems differs significantly from straight H_2 physisorption on non-metal-loaded supports. Platinum and nickel are interesting metals for spillover as they are capable of adsorbing hydrogen dissociatively and thereby acting as a source of hydrogen atoms to migrate onto the substrate surface. Likewise, palladium can both chemisorb atomic hydrogen and also dissolve it to form bulk hydride phases.[12,17] Supported Pd nanoparticles are also relevant as catalysts for organic and industrial reactions ranging from the low-temperature reduction of automobile pollutants,[18] general hydrogenations and dehydrogenations,[19] to C−C bond forming reactions[20] such as Heck,[21] Stille,[22] Suzuki,[23] and Sonogashira couplings.[24] It is important for many of these applications that the nanoparticles should be small in size and well-dispersed on a robust support of high surface area. Indeed a conceptually similar system, utilizing palladium nanoparticles supported by high-surface-area hyper-cross-linked polystyrene, was shown to give effective catalytic activity and selectivity.[25] Likewise, it was also shown that platinum supported by a covalent triazine-based framework was able to provide highly active low-temperature catalysis for methane oxidation by SO_3.[26] Recently, it was demonstrated that conjugated microporous polymer systems are able to function as effective support and stabilisation substrates for active metal nanoparticles, such as palladium.[27]

We target here systems based on a conjugated microporous polymer (CMP)[28] as the support material. There are rather few approaches for the direct synthesis of interconnected microporous organic polymers with high specific surface areas ($> 1000\ m^2/g$). We have previously described the synthesis of a range of amorphous conjugated microporous polymers (CMPs).[10b,28a,29] These CMP networks have a tunable micropore size distribution and surface area which is controlled by the length of the rigid organic linkers.[10b] CMPs are relatively thermally robust and chemically stable. We also recently demonstrated that it is possible to prepare CMP networks incorporating a range of chemical functionalities.[30] Hence, the surface groups and functionality of such polymer systems can be easily tailored for different applications.

We report here the impregnation of a conjugated poly(aryleneethynylene) polymer with palladium nanoparticles. We use supercritical CO_2 ($scCO_2$) as a solvent for the impregnation of a CMP network (CMP-0)[10b] with a CO_2-soluble palladium complex. Subsequent decomposition of the complex forms palladium nanoparticles within the CMP network. Supercritical fluid processing has been shown previously to be a useful method for generating metal nanoparticles in porous or polymeric materials that would be difficult to process with other techniques such as chemical vapor deposition (CVD) or solvent infusion.[31]

(15) (a) Li, Y. W.; Yang, R. T. *AIChE J*. **2008**, *54*(1), 269–279. (b) Li, Y. W.; Yang, R. T. *J. Phys. Chem. C* **2007**, *111*(29), 11086–11094. (c) Li, Y. W.; Yang, F. H.; Yang, R. T. *J. Phys. Chem. C* **2007**, *111*(8), 3405–3411. (d) Li, Y. W.; Yang, R. T. *J. Am. Chem. Soc*. **2006**, *128*(3), 726–727. (e) Li, Y. W.; Yang, R. T. *J. Phys. Chem. B* **2006**, *110*(34), 17175–17181. (f) Li, Y. W.; Yang, R. T. *J. Am. Chem. Soc*. **2006**, *128* (25), 8136–8137.

(16) Tsao, C. S.; Yu, M. S.; Chung, T. Y.; Wu, H. C.; Wang, C. Y.; Chang, K. S.; Chent, H. L. *J. Am. Chem. Soc*. **2007**, *129*(51), 15997–16004.

(17) Kiraly, Z.; Mastalir, A.; Berger, F.; Dekany, I. *Langmuir* **1997**, *13* (3), 465–468.

(18) Nishihata, Y.; Mizuki, J.; Akao, T.; Tanaka, H.; Uenishi, M.; Kimura, M.; Okamoto, T.; Hamada, N. *Nature* **2002**, *418*(6894), 164–167.

(19) (a) Astruc, D.; Lu, F.; Aranzaes, J. R. *Angew. Chem., Int. Ed*. **2005**, *44*(48), 7852–7872. (b) Solodenko, W.; Wen, H. L.; Leue, S.; Stuhlmann, F.; Sourkouni-Argirusi, G.; Jas, G.; Schonfeld, H.; Kunz, U.; Kirschning, A. *Eur. J. Org. Chem*. **2004**, No. 17, 3601–3610.

(20) Reetz, M. T.; Westermann, E. *Angew. Chem., Int. Ed*. **2000**, *39*(1), 165–+.

(21) (a) Farina, V. *Adv. Synth. Catal*. **2004**, *346*(13-15), 1553–1582. (b) Reetz, M. T.; de Vries, J. G. *Chem. Comm*. **2004**, No. 14, 1559–1563.

(22) Garcia-Martinez, J. C.; Lezutekong, R.; Crooks, R. M. *J. Am. Chem. Soc*. **2005**, *127*(14), 5097–5103.

(23) (a) Li, Y.; Hong, X. M.; Collard, D. M.; El-Sayed, M. A. *Org. Lett*. **2000**, *2*(15), 2385–2388. (b) Narayanan, R.; El-Sayed, M. A. *J. Catal*. **2005**, *234*(2), 348–355.

(24) Sawoo, S.; Srimani, D.; Dutta, P.; Lahiri, R.; Sarkar, A. *Tetrahedron* **2009**, *65*(22), 4367–4374.

(25) (a) Sidorov, S. N.; Volkov, I. V.; Davankov, V. A.; Tsyurupa, M. P.; Valetsky, P. M.; Bronstein, L. M.; Karlinsey, R.; Zwanziger, J. W.; Matveeva, V. G.; Sulman, E. M.; Lakina, N. V.; Wilder, E. A.; Spontak, R. J. *J. Am. Chem. Soc*. **2001**, *123*(43), 10502–10510. (b) Bykov, A.; Matveeva, V.; Sulman, M.; Valetskiy, P.; Tkachenko, O.; Kustov, L.; Bronstein, L.; Sulman, E. *Catal. Today* **2009**, *140*(1-2), 64–69. (c) Lyubimov, S. E.; Vasil'ev, A. A.; Korlyukov, A. A.; Ilyin, M. M.; Pisarev, S. A.; Matveev, V. V.; Chalykh, A. E.; Zlotin, S. G.; Davankov, V. A. *React. Funct. Polym*. **2009**, *69*(10), 755–758.

(26) Palkovits, R.; Antonietti, M.; Kuhn, P.; Thomas, A.; Schuth, F. *Angew. Chem., Int. Ed*. **2009**, *48*(37), 6909–6912.

(27) Schmidt, J.; Weber, J.; Epping, J. D.; Antonietti, M.; Thomas, A. *Adv. Mater*. **2009**, *21*(6), 702–705.

(28) (a) Jiang, J. X.; Su, F.; Trewin, A.; Wood, C. D.; Campbell, N. L.; Niu, H.; Dickinson, C.; Ganin, A. Y.; Rosseinsky, M. J.; Khimyak, Y. Z.; Cooper, A. I. *Angew. Chem. Int. Edit*. **2007**, *46*, 8574–8578. (b) Cooper, A. I. *Adv. Mater*. **2009**, *21*(12), 1291–1295.

(29) (a) Jiang, J. X.; Su, F.; Niu, H.; Wood, C. D.; Campbell, N. L.; Khimyak, Y. Z.; Cooper, A. I. *Chem. Comm*. **2008**, 486–488. (b) Jiang, J. X.; Su, F.; Trewin, A.; Wood, C. D.; Niu, H.; Jones, J. T. A.; Khimyak, Y. Z.; Cooper, A. I. *J. Am. Chem. Soc*. **2008**, *130*(24), 7710–7720. (c) Stoeckel, E.; Wu, X.; Trewin, A.; Wood, C. D.; Clowes, R.; Campbell, N. L.; Jones, J. T. A.; Khimyak, Y. Z.; Adams, D. J.; Cooper, A.I. *Chem. Comm*. **2009**, 212–214. (d) Jiang, J.-X.; Trewin, A.; Su, F.; Wood, C. D.; Niu, H.; Jones, J. T. A.; Khimyak, Y. Z.; Cooper, A. I. *Macromolecules* **2009**, *42*, 2658–2666.

(30) Dawson, R.; Laybourn, A.; Clowes, R.; Khimyak, Y. Z.; Adams, D. J.; Cooper, A. I. *Macromolecules* **2009**, *42*(22), 8809–8816.

(31) (a) Zhang, Y.; Erkey, C. *J. Supercrit. Fluids* **2006**, *38*(2), 252–267. (b) Woods, H. M.; Silva, M.; Nouvel, C.; Shakesheff, K. M.; Howdle, S. M. *J. Mater. Chem*. **2004**, *14*(11), 1663–1678. (c) Hasell, T.; Lagonigro, L.; Peacock, A. C.; Yoda, S.; Brown, P. D.; Sazio, P. J. A.; Howdle, S. M. *Adv. Funct. Mater*. **2008**, *18*(8), 1265–1271. (d) Cooper, A. I. *Adv. Mater*. **2001**, *13*(14), 1111–1114. (e) Furno, F.; Morley, K. S.; Wong, B.; Sharp, B. L.; Arnold, P. L.; Howdle, S. M.; Bayston, R.; Brown, P. D.; Winship, P. D.; Reid, H. J. *J. Antimicrob. Chemother*. **2004**, *54*(6), 1019–1024. (f) Morley, K. S.; Marr, P. C.; Webb, P. B.; Berry, A. R.; Allison, F. J.; Moldovan, G.; Brown, P. D.; Howdle, S. M. *J. Mater. Chem*. **2002**, *12*(6), 1898–1905. (g) Yang, J. X.; Hasell, T.; Smith, D. C.; Howdle, S. M. *J. Mater. Chem*. **2009**, *19*(45), 8560–8570.

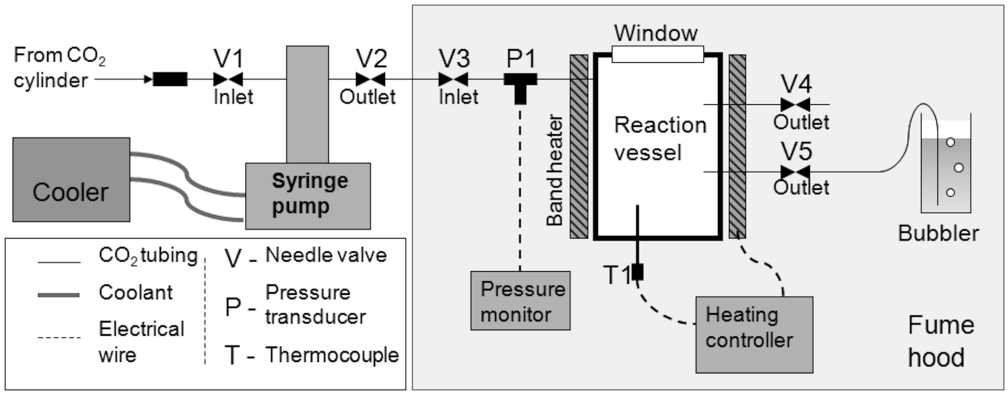

Figure 1. Schematic representation of the equipment used for the supercritical impregnation. The reaction vessel consists of a 10 mL volume stainless steel autoclave fitted with a sapphire view window.

The zero surface tension of $scCO_2$ permits better penetration and wetting of pores than liquid solvents and the solvent strength can be controlled by adjusting the CO_2 density. Simple removal from the substrate by depressurisation avoids problems of solvent residues or pore collapse on drying.[32] We show that $scCO_2$ processing is a viable route to introduce well-dispersed Pd nanoparticles throughout the conjugated microporous polymer matrix. The resultant materials are shown to exhibit enhanced hydrogen uptake in comparison with the unloaded polymer.

2. Experimental Methods

2.1. Chemicals. 1,3,5-Triethynylbenzene, 1,3,5-tris-(4-iodophenyl)benzene, tetrakis(triphenylphosphine)palladium(0), copper(I) iodide, palladium(II) hexafluoroacetylacetonate, palladium(II) acetylacetonate, and solvents were all purchased from Sigma-Aldrich and used as received. Carbon dioxide was purchased from BOC as supercritical fluid grade.

2.2. Synthesis of CMP-0. The support polymer network was synthesized by palladium catalyzed Sonogashira-Hagihara cross-coupling polycondensation, as reported previously.[10b] Briefly, 1,3,5-triethynylbenzene (450.5 mg, 3 mmol), 1,3,5-tris(4-iodophenyl)benzene (1368 mg, 2.0 mmol), tetrakis(triphenylphosphine)palladium(0) (80 mg), and copper(I) iodide (30 mg) were dissolved in a mixture of toluene (2.5 mL) and Et_3N (2.5 mL). The reaction mixture was heated to 80 °C and stirred for 72 h under a nitrogen atmosphere to rigorously exclude oxygen and to prevent homocoupling of the alkyne monomers. The network, a brown powder, was observed to precipitate from solution. The mixture was cooled to room temperature, and the network polymer was filtered and washed four times (once each) with chloroform, water, methanol, and acetone to remove any unreacted monomer or catalyst residues. The product was dried in vacuum for 24 h at 70 °C. Yield: 67.3%. IR (KBr, cm^{-1}): 3297.6 (−C′C−H), 2201.7 (−C′C−). Anal. Calcd for $C_{36}H_{18}$: C, 95.25; H, 4.75. Found: C, 86.15; H, 4.41. Apparent BET surface area = 998 m^2/g. The polymer morphology consisted of microparticulate rods and spheres, of ~1−5 μm diameter (see the Supporting Information), as described previously.

2.3. Impregnation of Nanoparticles. CMP-0 and palladium complex (either palladium(II) acetylacetonate or palladium(II) hexafluoroacetylacetonate) were placed in a stainless steel autoclave (10 mL) in separate glass vials. The polymer to palladium complex ratio used was 1:1 by mass (200 mg of each). The autoclave was then heated to 40 °C and pressurized with CO_2, using the equipment set up shown in Figure 1. A range of impregnations were performed at reaction pressures from 5.5 to 27.6 MPa. The autoclave was maintained at pressure for 2 h to allow equilibrium infusion to be reached, before being carefully depressurized at 40 °C over 5 min. The resultant product was then heated to 310 °C under nitrogen for 3 h to decompose the metal complex, before being subjected to dynamic vacuum at 120 °C for ~12 h to remove any remaining dissociated ligands.

2.4. Electron Microscopy (EM). Imaging of the palladium loaded polymer morphology was achieved using a Hitachi S-4800 cold Field Emission Scanning Electron Microscope (FE-SEM) operating in both scanning and transmission modes. The dry samples were prepared by dispersing the polymer powder into a methanol suspension and depositing onto carbon coated copper grids (300 mesh). The FE-SEM measurement scale bar was calibrated using certified SIRA calibration standards. Imaging was conducted at a working distance of 7 mm and a working voltage of 30 kV. Scanning images were taken using a combination of both upper and lower detector signals.

2.5. Thermogravimetric Analysis (TGA). TGA was carried out in platinum pans using a Q5000IR analyzer (TA Instruments) with an automated vertical overhead thermobalance. The samples were heated at 5 °C/min to 1000 °C under nitrogen and maintained at this temperature until the mass became stable.

2.6. Gas Sorption Analysis. Surface areas and pore widths were measured by nitrogen adsorption and desorption at 77.3 K using a Micromeritics ASAP 2020 volumetric adsorption analyzer. Samples were degassed by heating to 110 °C at 10°C/min and holding for 15 h under dynamic vacuum (10^{-5} bar) before analysis. Hydrogen isotherms were measured at room temperature up to 1.13 bar using a Micromeritics ASAP 2020 volumetric adsorption analyzer fitted with a water circulating bath to keep a constant temperature of 20 °C. The degas procedure for hydrogen sorption consisted of heating at 10 °C/min to 90 °C until < 10 μmHg vacuum pressure was reached and holding for 20 min, before heating to 300 °C at 10 °C/min and holding for 300 min. The sample was then transferred to the analysis port and degassed for a further 12 h at 300 °C. The non-heat-treated CMP-0 sample was degassed at the lower temperature of 120 °C so as not to cause changes to the structure arising from heating.

(32) Erkey, C. *J. Supercrit. Fluids* **2009**, *47*(3), 517–522.

Surface area was calculated from the N_2 adsorption isotherm using the BET method. Micropore surface area was calculated from the N_2 adsorption isotherm using the *t*-plot method. Micropore volume was derived using the *t*-plot method based on the Halsey thickness equation. Median pore width was determined based on Horvath−Kawazoe equation and the adsorption average pore width (4 V/A, from BET).

2.7. Solid-State NMR. Experiments were conducted at 9.4 T using a Bruker DSX-400 spectrometer operating at 400.13 and 100.61 for ^{1}H and ^{13}C respectively. Samples were spun in zirconia rotors driven by N_2 gas using a 4 mm ^{1}H/X/Y commercial probehead. ^{1}H−^{13}C Cross Polarisation Magic Angle Spinning (CP/MAS) NMR experiments were carried out at MAS of 10.0 kHz. The ^{1}H $\pi/2$ pulse was 3.1 μs and two pulse phase modulation (TPPM) decoupling[33] was used during the acquisition. The Hartmann-Hahn condition was set using hexamethylbenzene. The spectra were measured using contact time of 2.0 ms and relaxation delay of 10.0 s. Typically, 2048 scans were accumulated. The values of chemical shift are referred to TMS.

2.8. Powder X-ray Diffraction (PXRD). Data was measured using a PANalytical X'Pert PRO diffractometer with Cu−$K_{\alpha 1+2}$ radiation. The materials in the form of loose powders were mounted on a zero background holder and placed on a spinner stage (rotation of 2 cycles per second). The patterns were recorded in Bragg-Brentano reflection geometry and measured in the 25−60 2θ range. The particle sizes were determined using the Scherrer equation functionality within the X'Pert HighScore Plus software.

3. Results and Discussion

To prepare palladium nanoparticles within a polymer network, impregnation of palladium complexes into CMP-0 was attempted at a range of CO_2 pressures. Palladium(II) acetylacetonate was found to have insufficient solubility in CO_2 for effective impregnation[34] (see the Supporting Information), but the fluorinated analogue, palladium(II) hexafluoroacetylacetonate, was found to be sufficiently soluble. This is due to the presence of perfluorinated structure, as described elsewhere.[35] The mass increase of the polymer after impregnation demonstrates the efficiency of the loading (see Figure 2). The optimum pressure was found to be ~8 MPa, just above the critical pressure of CO_2, 7.38 MPa. This can be explained by two competing factors: solubility and solid−fluid partitioning. At lower pressures, the Pd complex is not soluble enough to be effectively transported into the polymer, whereas at higher pressures, the solubility increases to the point that the Pd complex preferentially partitions into the CO_2 outside of the polymer.

Decomposition of the palladium complex was then carried out by heating the sample to 310 °C. The mass of Pd in the polymer after decomposition of the Pd complex was determined by thermogravimetric analysis (TGA). These measurements were found to compare well

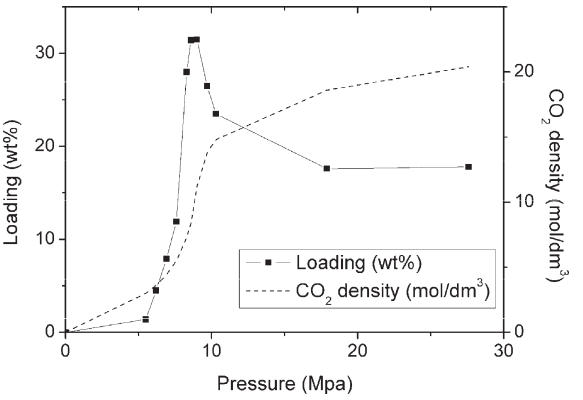

Figure 2. Loading of Pd complex as a function of CO_2 pressure at 40 °C.

with the theoretical loading calculated from the increase in mass of the polymer after impregnation, assuming complete loss of the ligands (see Figure 3A) upon heating. A decomposition temperature of 210 °C was chosen initially, well above a published condition of 150 °C for the decomposition of the palladium complex to form nanoparticles.[36] However, this was found to be insufficient to fully decompose the metal complex and remove the ligands, possibly due to stabilising effects imparted by the polymer substrate. The decomposition temperature was therefore raised to 310 °C for 3 h, as this was found by TGA to be sufficient to fully decompose the Pd complex (see Figure 3B). The neat organometallic complex, with no polymer support, is volatalized in the TGA at low temperatures (< 100 °C), leaving no residual Pd mass. After the Pd complex is loaded into the polymer, no such volatalization takes place and no mass is lost at equivalent temperatures. Rather, the Pd complex remains intact up to higher temperatures (< 290 °C), where it is presumably decomposed to Pd and dissociated ligands, as evidenced by the loss of mass (the ligands) above this temperature. A possible chemical alternative to this thermal reduction methods would be to chemically reduce the palladium complex using hydrogen, nonetheless thermal treatment was preferred for reasons of simplicity. It is also possible that improved contact between the polymer and metal nanoparticles might be achieved by thermal treatment, thus providing bridging sites for enhanced hydrogen spillover, as was suggested by Lachawiec et. al.[37]

The molecular level structure of CMP-0 was confirmed using solid state NMR and this was consistent with previous results.[10b] The parent palladium complex shows four sharp resonances at ca. 95, 115.4, 176.4, and 179.9 ppm. The resonances at 95.0 and 115.4 ppm correspond to the C−H and CF_3 of the triflouroacetyl acetonate, respectively. The two peaks at 174.4 and 179.9 ppm are a result of the quaternary carbon environments bound to oxygen. The spectra of CMP-0 after impregnation shows the presence of the palladium complex and its absence after decomposition as a result of heating (see Figure 4). The

(33) Hatton, B. D.; Landskron, K.; Hunks, W. J.; Bennett, M. R.; Shukaris, D.; Perovic, D. D.; Ozin, G. A. *Mater. Today* **2006**, *9*(3), 22–31.
(34) Yoda, S.; Mizuno, Y.; Furuya, T.; Takebayashi, Y.; Otake, K.; Tsuji, T.; Hiaki, T. *J. Supercrit. Fluids* **2008**, *44*(2), 139–147.
(35) Shezad, N.; Oakes, R. S.; Clifford, A. A.; Rayner, C. M. *Tetrahedron Lett.* **1999**, *40*(11), 2221–2224.
(36) Zhao, X.; Hirogaki, K.; Tabata, I.; Okubayashi, S.; Hori, T. *Surf. Coat. Technol.* **2006**, *201*(3-4), 628–636.
(37) Lachawiec, A. J.; Qi, G. S.; Yang, R. T. *Langmuir* **2005**, *21*(24), 11418–11424.

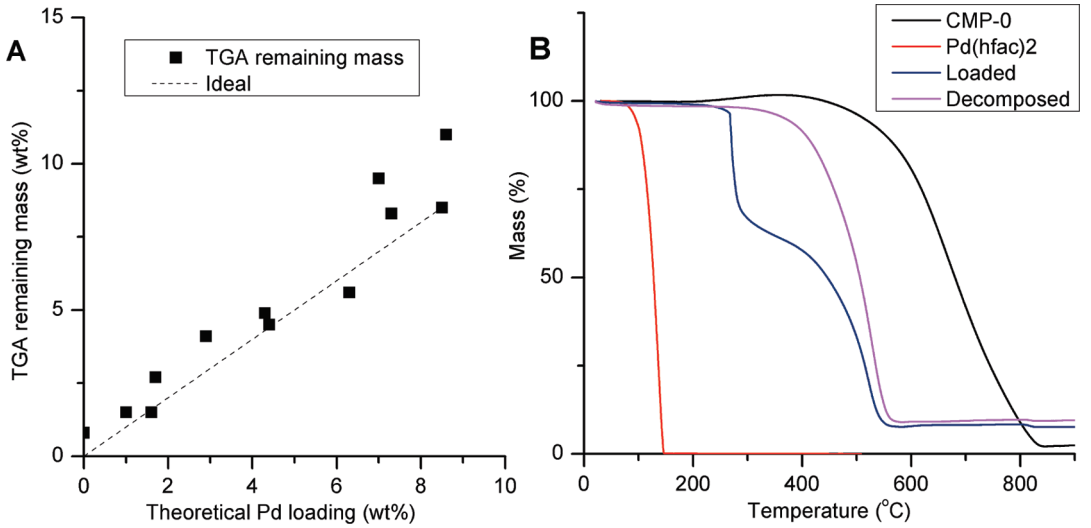

Figure 3. TGA: (A) The mass of Pd in the polymer products after impregnation and thermal treatment, determined as the remaining mass by TGA, compared to the theoretical mass calculated from the increase in mass after impregnation. The ideal value is indicated by the dashed line. (B) Comparison of the Pd complex, unmodified polymer, polymer after impregnation with Pd complex, and the same polymer after decomposition of the Pd complex to form nanoparticles. The decomposition step was carried out by heating to 310 °C for 3 h. It can be seen that after this step all the Pd complex had decomposed.

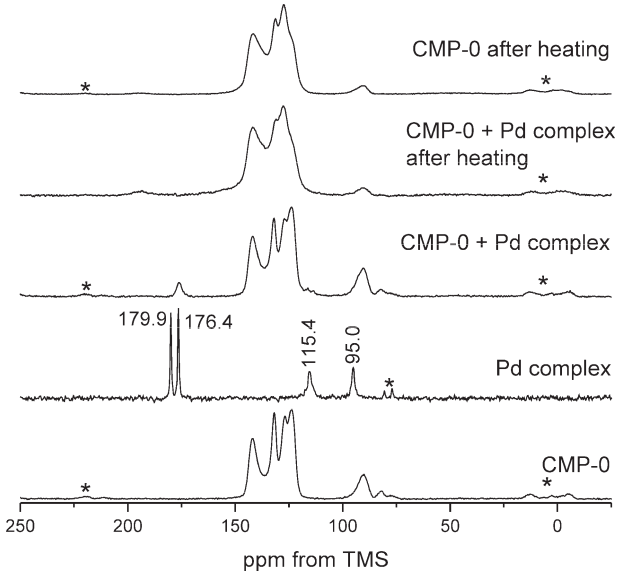

Figure 4. $^{1}H-^{13}C$ CP/MAS NMR spectra of the CMP-0 polymer networks recorded at a MAS rate of 10 kHz, asterisks denote spinning sidebands.

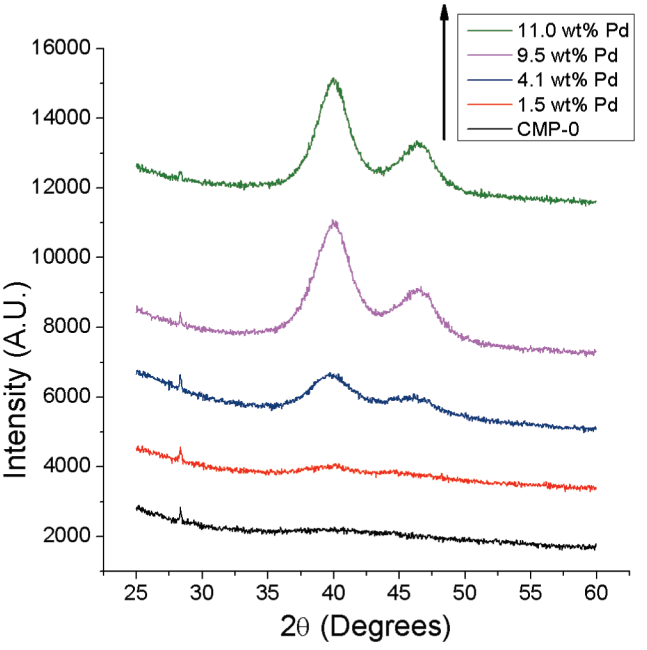

Figure 5. Powder XRD patterns for CMP-0 samples before and after incorporation of Pd nanoparticles. The intensity of the metallic Pd signal increases with the degree of metal loading into the polymer. The broad peak indicates that the Pd is present as small particles.

structure of the polymer is clearly affected by heating at the temperatures used in the decomposition step. The reduction in intensity of the terminal alkyne environment in the region of 75 to 85 ppm suggest further crosslinking occurs upon heating. However, there was little difference observed between unloaded CMP-0 heated in the same fashion and the heat-treated samples loaded with Pd. This suggests that the Pd does not strongly affect or catalyze thermal changes to the polymer.

Further evidence for the decomposition of the metal complex and the formation of elemental palladium was provided by powder XRD (see Figure 5). The diffraction patterns showed only amorphous material in the case of unloaded CMP-0, but showed a peak corresponding to metallic Pd in the case of the metal-loaded samples. The intensity of this peak increased markedly with increased gravimetric Pd incorporation. The peak width was broad because of the nanoparticulate nature of the Pd, and the crystallite was calculated using the Scherrer equation[38] (see Table 1). The average size of the nanoparticulate crystallites increased as the loading of Pd into the polymer was increased, in agreement with a higher concentration of metal allowing the growth of larger particles. Investigation of the products by scanning and transmission electron microscopy (see Figure 6) revealed larger nanoparticles on the surface of the polymer with smaller

(38) (a) Patterson, A. L. *Phys. Rev.* **1939**, *56*(10), 978–982. (b) Zhou, Y.; Dai, M. Z.; Ma, W. H.; Chen, X. M. *Chem. Eng. J.* **2009**, *150*(1), 237–241.

Table 1. Data for a Series of CMP-0 Polymer Samples, Unloaded and Pd-Loaded

sample	S_{BET} (m^2/g)[a]	S_{micro} (m^2/g)[b]	V_{total} (m^3/g)[c]	V_{micro} (m^3/g)[d]	pore width (Å)[e]	H_2 uptake (wt %)[f]	NP diameter (nm)[g]
CMP-0	1018	702	0.56	0.38	6.4	0.006	
CMP-0, heated	597	519	0.27	0.21	5.6	0.018	
Pd-CMP-0 4.1 wt %	306	250	0.17	0.10	7.2	0.033	3.3
Pd-CMP-0 9.5 wt %	604	259	0.36	0.11	6.7	0.069	3.8
Pd-CMP-0 11.0 wt %	652	113	0.44	0.06	7.9	0.062	4.32

[a] Surface area calculated from the N_2 adsorption isotherm using the BET method. [b] Micropore surface area calculated from the N_2 adsorption isotherm using the *t*-plot method. [c] Total pore volume at P/P_0) 0.99. [d] Micropore volume derived using the *t*-plot method based on the Halsey thickness equation. [e] Median pore width based on Horvath−Kawazoe equation. [f] Data were obtained at 0.113 MPa and 293.3 K. [g] Nanoparticle diameter based on the Scherrer equation applied to PXRD data.

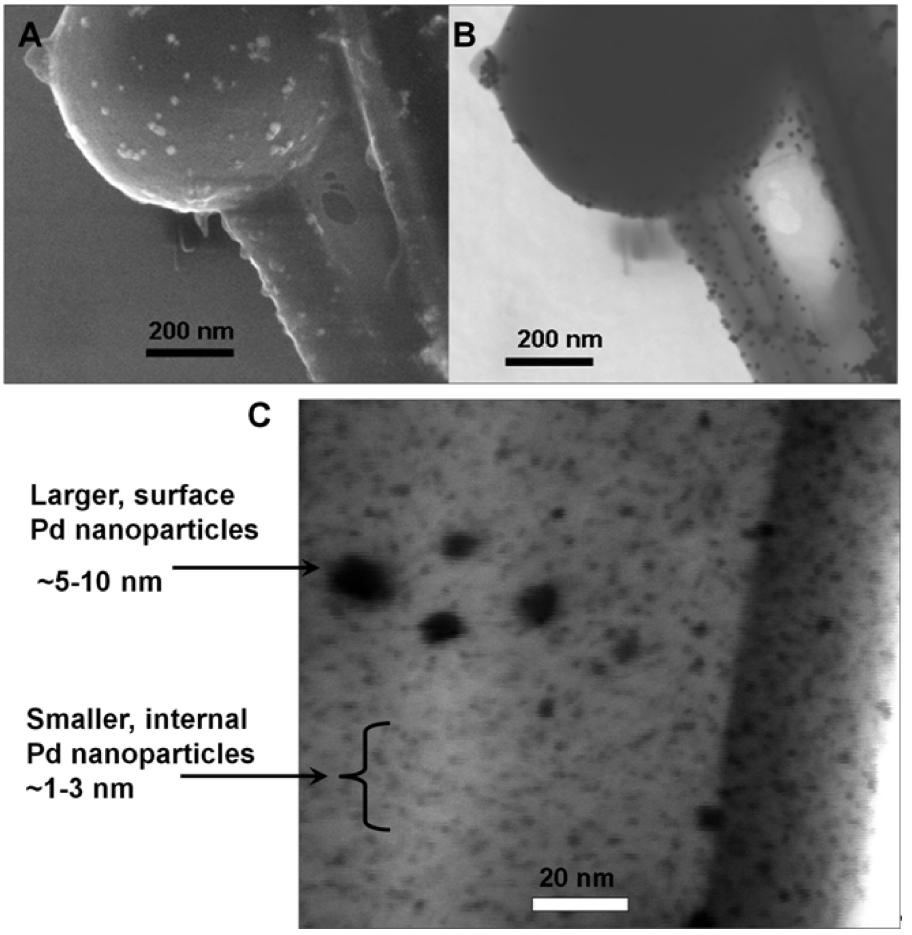

Figure 6. Electron microscopy of an 11.0 wt % Pd loaded CMP-0 sample. (A) Scanning mode image (left) and (B) transmission mode (right) of the same area of polymer. Both sphere and rod polymer morphologies are visible. At this magnification, only larger nanoparticles, which appear to be surface located, are visible. (C) Under higher-magnification transmission mode, a bimodal nanoparticle size distribution is observed.

nanoparticles being generated inside the polymer network. We ascribe the ~5−10 nm surface bound nanoparticles to Pd complex that is deposited on the surface during depressurisation. These particles are able to grow more freely, and hence agglomerate, whereas the growth of particles formed inside the microporous network is restricted by the pore dimensions. The nanoparticles inside the network were found to be ~1−3 nm in diameter, in close agreement with the average pore diameter of 2.4 nm, from the adsorption average pore width (4 V/A by BET). These particle sizes estimated from microscopy are in fair agreement with the estimated diameter from the PXRD data (Table 1), especially given that the Scherrer equation gives a weight rather than a number average. As such, the average size determined by the Scherrer equation would be expected to be slightly larger than the majority of the particles seen in TEM, as it will be skewed by the few larger surface particles. It is possible that the increase in nanoparticle size with Pd loading as seen by PXRD might be mostly a result of the surface nanoparticles that grow larger or more numerous as a function of complex loading, as opposed to the constrained nanoparticles inside the pores. Indeed, TEM suggests that at higher loading there is no noticeable increase in the size of the small internal particles, but that there is an increase in the size and number of larger surface particles (see the Supporting Information). The large number of smaller nanoparticles, as well as their dispersed nature throughout the small pores of the substrate, would be difficult to achieve with conventional impregnation techniques such

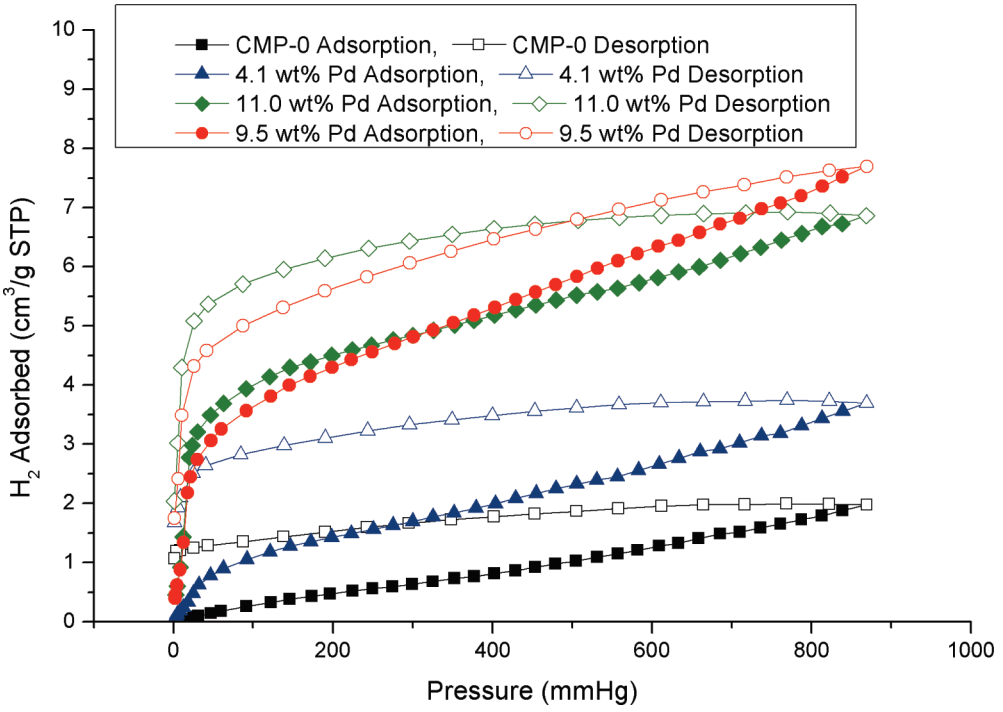

Figure 7. Low-pressure H_2 isotherms at 20 °C for the series of Pd-loaded samples. The hydrogen uptake is significantly increased by the inclusion of Pd nanoparticles, up to a maximum of 0.069 wt % H_2 for the 9.5 wt % loaded sample.

as solvent infusion or CVD.[32] This demonstrates the advantage of using supercritical CO_2 techniques for the generation of such materials.

A high degree of contact between Pd nanoparticles and the unsaturated microporous matrix was shown by others to induce a more efficient "pumping" of hydrogen out of the Pd−hydride phase and into the support.[12] For this reason, smaller nanoparticles and extensive dispersion are in principle desirable for increased spillover. Gas sorption measurements on the impregnated polymers studied here indicated that porosity was maintained after impregnation of Pd nanoparticles (Table 1). The total surface area and total pore volume of the heat treated samples were reduced in comparison to the unmodified CMP-0 materials, possibly as a result of partial collapse of some pores or contraction of the structure during heating. However, it was noted that the samples with higher Pd loadings retained more surface area and pore volume than the unloaded and low-loaded samples. A strong binding interaction between the electron rich conjugated moieties in the polymer and the electron deficient nanoparticle surface might explain this apparent "stabilization effect" of the nanoparticles towards thermal degradation of the polymer. The micropore volume decreases, and the pore width increases, with the incorporation of Pd nanoparticles (Table 1). This is as would be expected by the partial or complete blocking of narrower pores as the result of the growth of internal Pd nanoparticles, and is in agreement with other studies.[39] Hydrogen uptake at 293 K and 0.113 MPa was significantly enhanced by the addition of the Pd nanoparticles to the CMP-0 polymer (Figure 7 and Table 1). The highest H_2 uptake obtained, for the 9.5 wt % Pd loaded CMP-0, corresponded to 0.069 wt % hydrogen as compared to 0.018 wt % for CMP-0 in the absence of Pd impregnation. This is comparable with the uptake reported for similar metal-loaded porous systems under these conditions. For example, Pt on activated carbon gave 0.05 wt % uptake at room temperature and 1 atm pressure but this increased to ~1.2 wt % at 10 MPa.[15b] Pd nanoparticles on activated carbon fibres gave an uptake of ~0.025 wt % at room temperature and 1 atm pressure, which increased to 0.225 wt % at 2 MPa.[13] Finally, Pd nanoparticles on mesoporous ordered carbon has been recently shown to give an uptake of 0.083 wt % hydrogen at room temperature and 1 atm pressure, increasing to 0.58 wt % at 30 MPa.[39] It is interesting to note that the 11.0 wt % Pd loaded sample gave a higher hydrogen uptake at very low pressures, but a lower uptake than the 9.5 wt % Pd loaded sample by 1 atm. This highlights the compromise between incorporation of Pd, and conservation of the microporous structure of the material. The sharp initial increase in hydrogen uptake is attributed to adsorption directly to the metal, but higher loading reduces the micropore surface area and volume of the material (see Table 1), leading to a lower continued uptake at higher pressures. By comparison, a study by Yang et al. found the order of hydrogen uptake in Ru-doped template carbon to be 6 wt % > 8 wt % > 3 wt %. This was attributed to both the reduced surface area in the case of the 8 wt % sample and a lower amount of Ru metal as a dissociative hydrogen source in the case of the 3 wt % sample. Hence, the 6 wt % sample showed the highest uptake.[40] There is no evidence

(39) Saha, D.; Deng, S. *Langmuir* **2009**, *25*(21), 12550–12560.

(40) Wang, L. F.; Yang, R. T. *J. Phys. Chem. C* **2008**, *112*(32), 12486–12494.

in these studies that the CMP network behaves as a more efficient hydrogen acceptor than other comparable supports, for example as a result of the conjugation in the network backbone. We tentatively ascribe the sorption hysteresis observed for CMP-0 with no additional Pd loading to the presence of a small quantity of Pd in these samples as synthesized. This is due to residues from the Pd catalyst used in the cross-coupling reactions.[41] Indeed, previous EDX analysis of a series of similar CMP networks showed an entrained Pd content of between 1.03 and 3.94 wt % in the unloaded samples.[28a] Analysis of the unloaded CMP-0 by TGA shows a residual mass of 0.8 wt % when heated to 1000 °C under nitrogen, indicating that the total amount of entrained Pd and Cu combined does not exceed this figure.

4. Conclusions

Supercritical CO_2 has been shown to provide a simple and effective processing route to generate metal nanoparticle loaded conjugated microporous polymers. The nanoparticles are well dispersed throughout the material and show excellent size control within the pore matrix. Such polymer−metal composites materials may have future advantages over materials such as carbon because they can couple greater synthetic versatility with adequate thermal and chemical robustness. Microscopy and X-ray diffraction shows that the palladium nanoparticle size is confined by the narrow pore size distribution of the polymer network. Such systems may have potential as substrates for hydrogen spillover−for example, in catalytic processes−but the amounts of H_2 adsorbed at ambient temperature are very far below the levels that are interesting for practical gas storage applications. Future work will focus on the potential of these materials as stable and recyclable heterogeneous catalysts.

Acknowledgment. We are grateful to EPSRC (EP/C511794/1, EP/F057865/1) and the University of Liverpool for funding. A.I.C. holds a Royal Society Wolfson Research Merit Award. We thank Dr. E. Willneff for assistance with PXRD measurements.

Supporting Information Available: Solubility data for palladium complexes in $scCO_2$; additional SEM and TEM images and a nanoparticle size distribution histogram (PDF). This material is available free of charge via Internet at http://pubs.acs.org.

(41) Sonogashira, K.; Tohda, Y.; Hagihara, N. *Tetrahedron Lett*. **1975**, No. 50, 4467–4470.